Vol 458|12 March 2009|doi:10.1038/nature07853

LETTERS

Battery materials for ultrafast charging and discharging

Byoungwoo Kang[1] & Gerbrand Ceder[1]

The storage of electrical energy at high charge and discharge rate is an important technology in today's society, and can enable hybrid and plug-in hybrid electric vehicles and provide back-up for wind and solar energy. It is typically believed that in electrochemical systems very high power rates can only be achieved with supercapacitors, which trade high power for low energy density as they only store energy by surface adsorption reactions of charged species on an electrode material[1–3]. Here we show that batteries[4,5] which obtain high energy density by storing charge in the bulk of a material can also achieve ultrahigh discharge rates, comparable to those of supercapacitors. We realize this in $LiFePO_4$ (ref. 6), a material with high lithium bulk mobility[7,8], by creating a fast ion-conducting surface phase through controlled off-stoichiometry. A rate capability equivalent to full battery discharge in 10–20 s can be achieved.

Like any lithium battery material, $LiFePO_4$ absorbs and releases energy by the simultaneous extraction and, respectively, insertion of Li^+ ions and electrons. Hence, the power capability of a lithium battery with this or other electrode materials will depend critically on the rate at which the Li^+ ions and electrons can migrate through the electrolyte and composite electrode structure into the active electrode material. Strategies to increase the low rate performance of bulk $LiFePO_4$ have focused on improving electron transport in the bulk[9] or at the surface of the material[10,11], or on reducing the path length over which the electron and Li^+ ion have to move by using nano-sized materials[12,13]. However, recent evidence indicates that Li^+ transport along the surface may be as important as electron transport: whereas $LiFePO_4$ can in principle exchange Li^+ ions with the electrolyte on all surface facets, Li^+ ions can only move into the bulk of the crystal in the [010] direction[7,8,14]. Hence, increasing diffusion across the surface towards the (010) facet should enhance rate capability.

In a departure from previous approaches[9–11], we have created a lithium phosphate coating on the surface of nanoscale $LiFePO_4$ and show that this results in extremely high rate performance. In particular, glassy lithium phosphates are well known to be good, stable Li^+ conductors[15] and can be doped with transition metals to achieve electronic conduction[16–18]. Supplementary Fig. 1 shows a small section of the calculated lithium–iron–phosphorus ternary phase diagram[19] equilibrated with an oxygen potential under reducing conditions, which represents typical synthesis conditions for $LiFePO_4$. Compositions with high phosphorus content on the Li_2O–P_2O_5 binary edge are known to be very good glass formers with high lithium conductivity[20], and nitrogen-doped Li_3PO_4 has been used as a solid-state lithium electrolyte[15]. Typically, the glass-forming ability and lithium conductivity decrease with the presence of Li_2O. These glasses can dissolve a large quantity of transition-metal ions to increase the electronic conductivity[17,21], although such fully amorphous states with high levels of transition metals are usually only obtained by rapid quenching from the liquid state. Hence, the shaded area in the phase diagram represents the optimal coating compositions with good lithium ion conductivity.

Our synthesis strategy has been to create an appropriate off-stoichiometry in the starting materials so that the coating constituents phase-separate from $LiFePO_4$ as it forms during the heat treatment, thereby creating the active storage material and coating in a single process. Here we describe results with an iron:phosphorus deficiency ratio of 2:1 (for example $LiFe_{1-2y}P_{1-y}O_{4-\delta}$, $y = 0.05$), as indicated by arrow A in Supplementary Fig. 1. We note that the more common one-to-one iron:phosphorus deficiency (arrow B in Supplementary Fig. 1, equivalent to lithium excess[22]) creates a mixture of Li_3PO_4 and iron oxides, which are not likely to conduct well under the synthesis conditions used to prepare $LiFePO_4$.

$LiFe_{0.9}P_{0.95}O_{4-\delta}$ was synthesized by ball-milling Li_2CO_3, $FeC_2O_4 \cdot 2H_2O$ and $NH_4H_2PO_4$ in appropriate amounts, heating the mixture at 350 °C for 10 h and then heating at 600 °C for 10 h under argon. X-ray diffraction (Fig. 1a and Supplementary Fig. 2) shows that despite the off-stoichiometric starting mixture, stoichiometric $LiFePO_4$ forms with lattice parameters ($a = 10.3134$ Å, $b = 6.002$ Å and $c = 4.691$ Å) very similar to those reported in the literature[23]. No crystalline Fe_2P can be observed in the X-ray pattern of the material synthesized at 600 °C, but a small amount of Fe_2P is present in the material synthesized at 700 °C (Fig. 1a). However, amorphous FeP or Fe_2P created by the reducing atmosphere cannot be excluded[24]. Mössbauer spectroscopy (Supplementary Fig. 4) indicates that apart from the major $LiFePO_4$ component, around 10% of the Fe is present in some other environment. The isomer shift (0.464 mm s^{-1}) and quadrupole splitting (0.798 mm s^{-1}) of this second component fall in the region of values given in the literature for Fe^{3+} in pyrophosphate (P_2O_7-containing) glasses, although recent work[24] argues that iron monophosphides also give a Mössbauer signal in this range. To distinguish between the two possibilities, as-made material was discharged. The large discharge capacity found (Supplementary Fig. 5) is consistent with the presence of reducible Fe^{3+} rather than FeP in the material. Furthermore, in subsequent charge–discharge cycles we consistently find 15–18 mA h g^{-1} capacity in the 3.2–2.0 V voltage window, in agreement with the ~10% proportion of iron found in the second Mössbauer component. Pyrophosphates are known to have somewhat lower potential than $LiFePO_4$[25].

Particle size as determined by scanning electron microscopy is ~50 nm (Fig. 1b). Transmission electron microscopy (Fig. 1c) shows a poorly crystallized thin layer on the surface. The thickness of this layer varies. Further evidence for the existence of the poorly crystallized layer is provided by X-ray photoelectron spectroscopy, which selectively analyses the surface of a material, and shows two different phosphorus 2*p* chemical states in our material. One state is close to the phosphorus 2*p* binding energy in $LiFePO_4$, but the second component is at higher energy. This is consistent with the presence of the $(P_2O_7)^{4-}$ groups, where phosphorus has higher binding energy than $LiFePO_4$ (Fig. 2 and

[1]Department of Materials Science and Engineering, Massachusetts Institute of Technology, 77 Massachusetts Avenue, Cambridge, Massachusetts 02139, USA.

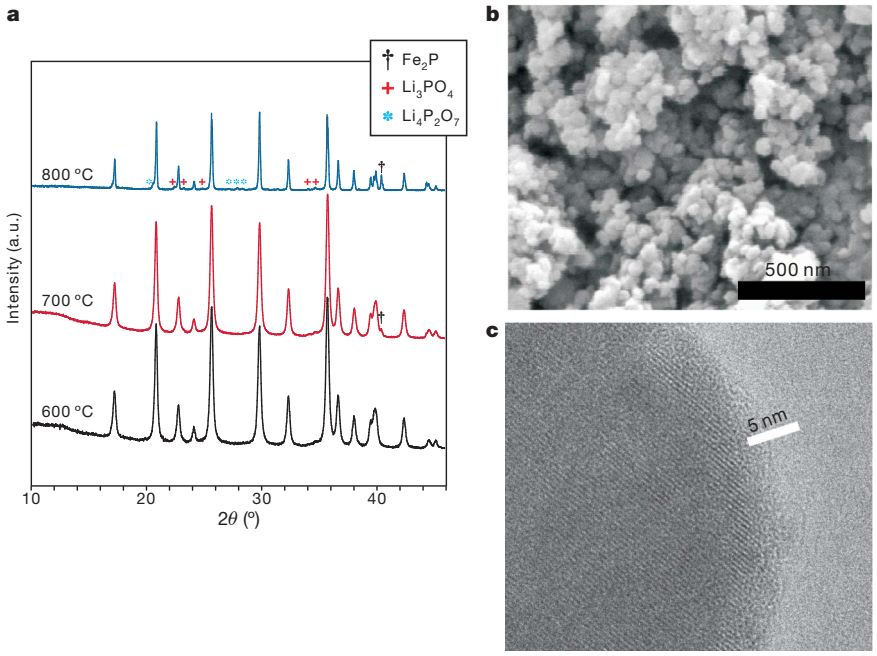

Figure 1 | Characterization of $LiFeP_{0.9}P_{0.95}O_{4-\delta}$ synthesized under argon. **a**, Powder X-ray diffraction patterns (using Cu Kα radiation) for samples synthesized at different temperatures. Fe_2P starts to appear at 700 °C and $Li_4P_2O_7$ starts to crystallize at 800 °C. The lattice parameters for the material synthesized at 600 °C are $a = 10.3134$ Å, $b = 6.002$ Å and $c = 4.691$ Å. θ, diffraction angle; a.u., arbitrary units. **b**, Scanning electron microscopy image showing a particle size of less than 50 nm. **c**, Transmission electron microscopy image of the material showing a poorly crystallized layer less than 5 nm thick on the edge of a particle.

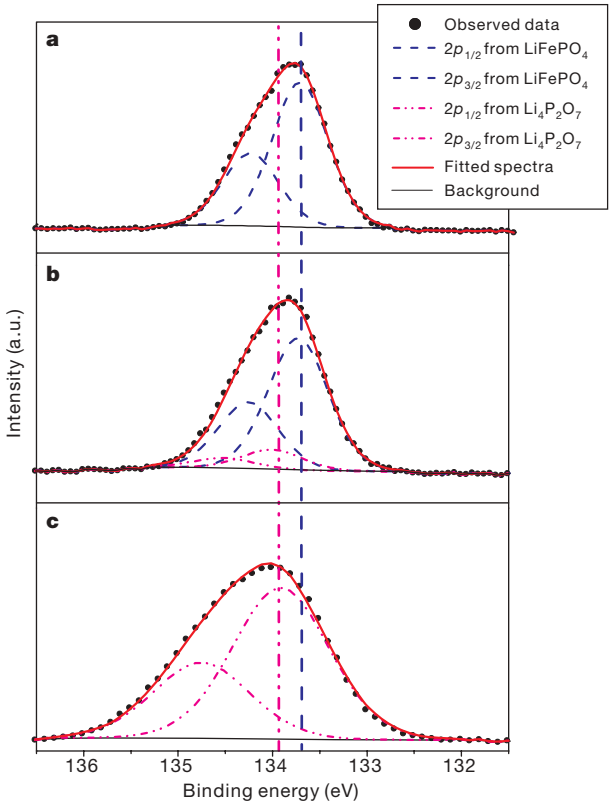

Figure 2 | Phosphorus 2*p* X-ray photoelectron spectra from three different compounds. **a**, $LiFePO_4$; **b**, $LiFe_{0.9}P_{0.95}O_{4-\delta}$; **c**, $Li_4P_2O_7$. The spectra were fitted to the phosphorus 2*p* doublet, $2p_{1/2}$ and $2p_{3/2}$, which is split by 0.84 eV in an integrated intensity ratio of 1:2. The higher energy, lower intensity peak is the $2p_{1/2}$ peak. $LiFe_{0.9}P_{0.95}O_{4-\delta}$ shows two different chemical states for phosphorus. The vertical blue dashed line is the phosphorus $2p_{3/2}$ peak from $LiFePO_4$ and the vertical pink dash–dot line is the phosphorus $2p_{3/2}$ peak from $Li_4P_2O_7$. The data were corrected on the basis of the binding energy of adventitious hydrocarbon, 248.8 eV. The fitted values are in Supplementary Table 1.

Supplementary Table 1)[26]. Elemental analysis of our materials synthesized at 600 °C, performed with scanning transmission electron microscopy (Supplementary Fig. 3), also indicates that the phosphorus:iron ratio on the surface is increased by introducing the off-stoichiometry in the sample. Together, the X-ray photoelectron spectroscopy, Mössbauer spectroscopy and scanning transmission electron microscopy data, as well as the starting stoichiometry, support the idea that the second phase present is a Fe^{3+}-containing $Li_4P_2O_7$-like phase.

Swagelok cells with a metallic lithium anode were assembled to investigate the material. Figure 3a shows the discharge of the material at various rates after a slow charge and hold at 4.3 V to fully charge the material. A rate of *n*C corresponds to a full discharge in $1/n$ h. At a 2C rate, the material still discharges to its estimated theoretical capacity of ~166 mA h g^{-1}. (The theoretical capacity is calculated by assuming a mixture of $LiFePO_4$ and $Li_4P_2O_7$.) Even at the highest rate tested (50C), corresponding to a time of 72 s to fully discharge the capacity, the material achieves about 80% of its theoretical capacity. Capacity retention of the material is superior. As Fig. 3b shows, after 50 full charge–discharge cycles at rates of 20C and 60C, there is no significant capacity loss.

For an electrochemical cell to deliver energy at high rate, all parts of the Li^+–electron path between the anode and cathode active material have to be capable of sustaining this rate. The results in Fig. 3 were obtained when testing a standard cathode preparation using 15 wt% carbon black and 5 wt% polyethylenetetrafluoride as binder. Carbon black is added to facilitate electron transport from the active materials to the current collector. As this preparation has been optimized for materials that have substantially lower rates (~1C) we also tested preparations with up to 65 wt% carbon. Although such high carbon loadings are inappropriate for real batteries, they are useful in establishing the true rate capability of the active material and are commonly used in the testing of high-rate nanomaterials[13,18,27]. The results in Fig. 4 show that extremely high rates can be achieved for the active material: at a 200C rate (corresponding to an 18-s total discharge) more than 100 mA h g^{-1} can still be achieved, and a capacity of 60 mA h g^{-1} is obtained at a 400C rate (9 s to full discharge). Such discharge rates are two orders of magnitude larger than those used in today's lithium ion batteries.

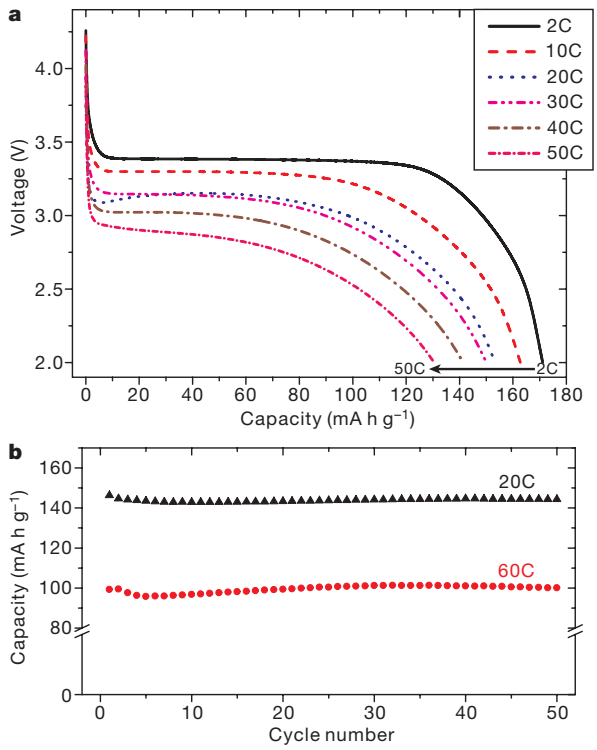

Figure 3 | Discharge rate capability and capacity retention for $LiFe_{0.9}P_{0.95}O_{4-\delta}$ synthesized at 600 °C. **a**, Discharge rate capability after charging at C/5 and holding at 4.3 V until the current reaches C/60. C/*n* denotes the rate at which a full charge or discharge takes *n* hours. The loading density of the electrode is 3.86 mg cm^{-2}. At 2C, the capacity is close to the theoretical value. **b**, Capacity retentions when performing full charge–discharge cycles at constant 20C and 60C current rates for 50 cycles. The loading density of the electrode is 3.60 mg cm^{-2} for the 20C rate and 2.71 mg cm^{-2} for the 60C rate. The voltage window is approximately 2.5–4.3 V. The electrode formulation is active material (80 wt%), carbon (15 wt%) and binder (5 wt%).

Our work provides evidence that extremely high electrochemical discharge rates can be achieved with lithium battery materials. Typical power rates for lithium ion battery materials are in the range of 0.5 to 2 kW kg^{-1}. The specific power we observed for the modified $LiFePO_4$ (170 kW kg^{-1} at a 400C rate and 90 kW kg^{-1} at a 200C rate) is two orders of magnitude higher, but consistent with the very high lithium diffusivity estimated earlier from theoretical calculations[7,8]. Taking the estimated value of the lithium diffusion constant in the [010] direction to be $\sim 10^{-8}$ cm^2 s^{-1}, from ref. 8, we estimate the time for Li^+ to diffuse over 50 nm (approximate particle size) to be [50 nm]^2/[10^{-8} cm^2 s^{-1}], that is, <1 ms. Hence, the limiting factor for charge/discharge is the delivery of Li^+ and electrons to the surface rather than bulk diffusion. This may explain the success of our strategy to facilitate transport across the surface by creating a poorly crystallized layer with high Li^+ mobility. The amorphous nature of the coating removes the anisotropy of the surface properties[28] and enhances delivery of Li^+ to the (010) facet of $LiFePO_4$ where it can be inserted.

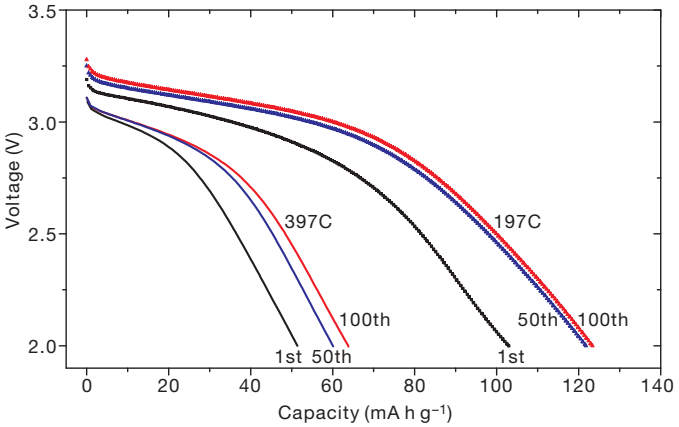

Figure 4 | Discharge capability at very high rate for $LiFe_{0.9}P_{0.95}O_{4-\delta}$ synthesized at 600 °C. Full charge–discharge cycles at constant 197C and 397C current rates without holding the voltage. The loading density of the electrode is 2.96 mg cm^{-2}. The first, fiftieth and hundredth discharges are shown for each rate. The electrode formulation is active material (30 wt%), carbon black (65 wt%) and binder (5 wt%).

It is also plausible that the disordered nature of the coating material modifies the surface potential of lithium to facilitate the adsorption of Li^+ from the electrolyte by providing different lithium sites with a wide range of energies that can be matched to the energy of lithium in the electrolyte. The fact that the particles of our material are nano-sized definitely contributes to its extreme discharge rate capability, but its performance is substantially better than results reported in the literature for particles of similar[9] or smaller size[13], indicating that the coating also enhances the rate capability. To further test that the pyrophosphate coating is responsible for the ultrahigh power rate, we evaluated stoichiometric $LiFePO_4$ synthesized under the same conditions. In this case, the precursors were ball-milled so that grain size after sintering would be the same as for the off-stoichiometric material (Supplementary Fig. 6a). Although the rate capability of this material is good, it is clearly inferior to the off-stoichiometric material (Supplementary Fig. 6b).

Because limited electron transport through the electrode assembly can mask the true rate capability of the material[29,30], our highest rates (200C and 400C) could only be tested with large amounts of carbon, which reduces the volumetric energy density of the electrode. This problem can be addressed by developing electrode structures with good electronic conductivity and percolation while optimizing the volume fraction of the active energy-storing component.

The ability to charge and discharge batteries in a matter of seconds rather than hours may make possible new technological applications and induce lifestyle changes. Such changes may first take place in the use of small devices, where the total amount of energy stored is small. Only 360 W is required to charge a 1 W h cell phone battery in 10 s (at a 360C charging rate). On the other hand, the rate at which very large batteries such as those planned for plug-in hybrid electric vehicles can be charged is likely to be limited by the available power: 180 kW is needed to charge a 15 kW h battery (a typical size estimated for a plug-in hybrid electric vehicle) in 5 min.

Electrode materials with extremely high rate capability will blur the distinction between supercapacitors and batteries. The power density based on the measured volume of the electrode film, including carbon and binder, is around 65 kW l^{-1} in the 400C test. Assuming that the cathode film takes up about 40% of the volume of a complete cell, this will give a power density of $\sim$25 kW l^{-1} at the battery level, which is similar to or higher than the power density in a supercapacitor, yet with a specific energy and energy density one to two orders of magnitude higher. The fact that our material can obtain power densities similar to those of supercapacitors is consistent with there being an exceedingly fast bulk process. For $LiFePO_4$, bulk lithium transport is so fast that the charging is ultimately limited by the surface adsorption and surface transfer, which is also the rate-limiting step in supercapacitors.

METHODS SUMMARY

We synthesized the $LiFe_{1-2y}P_{1-y}O_{4-\delta}$ samples by solid-state reaction using Li_2CO_3 (Fisher Scientific company), $FeC_2O_4 \cdot 2H_2O$ (99.999%, Alfa Aesar) and $NH_4H_2PO_4$ (98%, Alfa Aesar). The mixture in the acetone was ball-milled and heated at 350 °C for 10 h under argon to decompose the carbonate, oxalate and ammonium. The sample was cooled to room temperature, ground and manually

pelletized under 10,000-lb pressure using a disk-shaped mould. After preheating, we heated the pellet at 600 °C for 10 h under argon. Electrodes were made by mixing active material (80 wt%), carbon (carbon black; 15 wt%) and binder (polyethylenetetrafluoride; 5 wt%). The very high rate tests (200C and 400C) were performed on electrodes with 30 wt% active material, 65 wt% carbon and 5 wt% binder. We assembled the cells in an argon-filled glove box and tested them on a Maccor 2200 operating in galvanostatic mode using lithium metal as an anode, non-aqueous electrolyte (1 M $LiPF_6$ in ethylene carbonate:dimethyl carbonate (1:1), Merck) and Celgard 2600 or 2500 as separator in a Swagelok cell. All cells were tested at room temperature.

Received 18 June 2007; accepted 2 February 2009.

1. Conway, B. E. Transition from supercapacitor to battery behavior in electrochemical energy-storage. *J. Electrochem. Soc.* **138,** 1539–1548 (1991).
2. Arico, A. S., Bruce, P., Scrosati, B., Tarascon, J. M. & Van Schalkwijk, W. Nanostructured materials for advanced energy conversion and storage devices. *Nature Mater.* **4,** 366–377 (2005).
3. Amatucci, G. G., Badway, F., Du Pasquier, A. & Zheng, T. An asymmetric hybrid nonaqueous energy storage cell. *J. Electrochem. Soc.* **148,** A930–A939 (2001).
4. Tarascon, J. M. & Armand, M. Issues and challenges facing rechargeable lithium batteries. *Nature* **414,** 359–367 (2001).
5. Reed, J. & Ceder, G. Role of electronic structure in the susceptibility of metastable transition-metal oxide structures to transformation. *Chem. Rev.* **104,** 4513–4533 (2004).
6. Padhi, A. K., Nanjundaswamy, K. S. & Goodenough, J. B. Phospho-olivines as positive-electrode materials for rechargeable lithium batteries. *J. Electrochem. Soc.* **144,** 1188–1194 (1997).
7. Islam, M. S., Driscoll, D. J., Fisher, C. A. J. & Slater, P. R. Atomic-scale investigation of defects, dopants, and lithium transport in the $LiFePO_4$ olivine-type battery material. *Chem. Mater.* **17,** 5085–5092 (2005).
8. Morgan, D., Van der Ven, A. & Ceder, G. Li conductivity in Li_xMPO_4 (M = Mn, Fe, Co, Ni) olivine materials. *Electrochem. Solid State Lett.* **7,** A30–A32 (2004).
9. Chung, S. Y., Bloking, J. T. & Chiang, Y. M. Electronically conductive phospho-olivines as lithium storage electrodes. *Nature Mater.* **1,** 123–128 (2002).
10. Ravet, N. C. Y., Magnan, J. F., Besner, S., Gauthier, M. & Armand, M. Electroactivity of natural and synthetic triphylite. *J. Power Sources* **97–8,** 503–507 (2001).
11. Herle, P. S., Ellis, B., Coombs, N. & Nazar, L. F. Nano-network electronic conduction in iron and nickel olivine phosphates. *Nature Mater.* **3,** 147–152 (2004).
12. Delacourt, C., Poizot, P., Levasseur, S. & Masquelier, C. Size effects on carbon-free $LiFePO_4$ powders. *Electrochem. Solid State Lett.* **9,** A352–A355 (2006).
13. Kim, D. H. & Kim, J. Synthesis of $LiFePO_4$ nanoparticles in polyol medium and their electrochemical properties. *Electrochem. Solid State Lett.* **9,** A439–A442 (2006).
14. Chen, G. Y., Song, X. Y. & Richardson, T. J. Electron microscopy study of the $LiFePO_4$ to $FePO_4$ phase transition. *Electrochem. Solid State Lett.* **9,** A295–A298 (2006).
15. Wang, B., Kwak, B. S., Sales, B. C. & Bates, J. B. Ionic conductivities and structure of lithium phosphorus oxynitride glasses. *J. Non-Cryst. Solids* **183,** 297–306 (1995).
16. Sayer, M. & Mansingh, A. Transport properties of semiconducting phosphate glasses. *Phys. Rev. B* **6,** 4629–4643 (1972).
17. Mogus-Milankovic, A., Santic, A., Karbulut, M. & Day, D. E. Study of electrical properties of MoO_3-Fe_2O_3-P_2O_5 and SrO-Fe_2O_3-P_2O_5 glasses by impedance spectroscopy. II. *J. Non-Cryst. Solids* **330,** 128–141 (2003).
18. Zhou, H. S., Li, D. L., Hibino, M. & Honma, I. A self-ordered, crystalline-glass, mesoporous nanocomposite for use as a lithium-based storage device with both high power and high energy densities. *Angew. Chem. Int. Edn Engl.* **44,** 797–802 (2005).
19. Ong, S. P., Wang, L., Kang, B. & Ceder, G. Li-Fe-P-O_2 phase diagram from first principles calculations. *Chem. Mater.* **20,** 1798–1807 (2008).
20. Martin, S. W. Ionic-conduction in phosphate-glasses. *J. Am. Ceram. Soc.* **74,** 1767–1784 (1991).
21. Sobha, K. C. & Rao, K. J. Investigation of phosphate glasses with the general formula $A_xB_yP_3O_{12}$ where A=Li, Na or K and B=Fe, Ga, Ti, Ge, V or Nb. *J. Non-Cryst. Solids* **201,** 52–65 (1996).
22. Kim, D.-K. *et al.* Effect of synthesis conditions on the properties of $LiFePO_4$ for secondary lithium batteries. *J. Power Sources* **159,** 237–240 (2006).
23. Ellis, B. *et al.* Nanostructured materials for lithium-ion batteries: Surface conductivity vs. bulk ion/electron transport. *Faraday Discuss.* **134,** 119–141 (2007).
24. Rho, Y. H., Nazar, L. F., Perry, L. & Ryan, D. Surface chemistry of $LiFePO_4$ studied by Mossbauer and X-ray photoelectron spectroscopy and its effect on electrochemical properties. *J. Electrochem. Soc.* **154,** A283–A289 (2007).
25. Padhi, A. K., Nanjundaswamy, K. S., Masquelier, C., Okada, S. & Goodenough, J. B. Effect of structure on the Fe^{3+}/Fe^{2+} redox couple in iron phosphates. *J. Electrochem. Soc.* **144,** 1609–1613 (1997).
26. Morgan, W. E., Stec, W. J. & Vanwazer, J. R. Inner-orbital photoelectron spectroscopy of alkali-metal halides, perchlorates, phosphates, and pyrophosphates. *J. Am. Chem. Soc.* **95,** 751–755 (1973).
27. Okubo, M. *et al.* Nanosize effect on high-rate Li-ion intercalation in $LiCoO_2$ electrode. *J. Am. Chem. Soc.* **129,** 7444–7452 (2007).
28. Wang, L., Zhou, F., Meng, Y. S. & Ceder, G. First-principles study of surface properties of $LiFePO_4$: Surface energy, structure, Wulff shape, and surface redox potential. *Phys. Rev. B* **76,** 165435 (2007).
29. Dominko, R., Gaberscek, M., Bele, A., Mihailovic, D. & Jamnik, J. Carbon nanocoatings on active materials for Li-ion batteries. *J. Eur. Ceram. Soc.* **27,** 909–913 (2007).
30. Gaberscek, M., Dominko, R., Bele, M., Remskar, M. & Jamnik, J. Mass and charge transport in hierarchically organized storage materials. Example: Porous active materials with nanocoated walls of pores. *Solid State Ionics* **177,** 3015–3022 (2006).

Supplementary Information is linked to the online version of the paper at www.nature.com/nature.

Acknowledgements B.K. thanks D. S. Yun and Y. Zhang for the help with transmission electron microscope measurements and K. Kang and Y. S. Meng for experimental help and discussions. Support from the US National Science Foundation through the Materials Research Science and Engineering Centers programme and the Batteries for Advanced Transportation Program of the US Department of Energy is gratefully acknowledged.

Author Contributions B.K. performed the experiments and G.C. supervised and analysed the work.

Author Information Reprints and permissions information is available at www.nature.com/reprints. Correspondence and requests for materials should be addressed to G.C. (gceder@mit.edu).